High-order additions to platinum-based alloys for high-temperature applications

by B.O. Odera*†‡§, M.J. Papo‡**, R. Couperthwaite**, G.O. Rading†§, D. Billing∞, and L.A. Cornish*†‡

Synopsis

Platinum-based alloys are being developed with microstructures similar to nickel-based superalloys for potential high-temperature applications in aggressive environments. Since the chemistries of nickel and platinum are similar, Pt-based alloys can be made with gamma prime ~Pt_3Al precipitates in a gamma (Pt) matrix. Currently, the Pt-Al-Cr-Ru system is one of the bases for developing Pt-based alloys, where Al allows the formation of the Pt_3Al precipitate and also gives protection from the alumina scale formed, Cr provides oxidation resistance and stabilization for the $L1_2$ ~Pt_3Al phase, and Ru provides solid solution strengthening in the (Pt) matrix.

Four Pt-Al-Cr-Ru-V and two Pt-Al-Cr-Ru-V-Nb alloys were made, with compositions based on a quaternary alloy, ~Pt_{82}:Al_{12}:Cr_4:Ru_2, which had previously been identified as having optimum properties. Four of the as-cast alloys had the targeted two-phase structure of ~Pt_3Al and (Pt), and two were single-phase ~Pt_3Al. Vanadium partitioned more to (Pt) than to ~Pt_3Al. There was an improvement in hardness compared to the quaternary alloys. The best addition of V was ~15 at.%; higher additions resulted in brittle intermetallic phases of the Pt-V system. The effect of Nb could not be ascertained because of its high losses.

Keywords
high-order Pt-based alloys, scanning electron microscopy, X-ray diffraction, microhardness.

Introduction

Although the nickel-based superalloys (NBSAs) have excellent mechanical properties at high temperatures, they are limited by their maximum application temperature, which is dictated by the melting point of the nickel solid-solution matrix. Currently, the maximum temperature at which NBSAs operate is about 1100°C, which is approximately 90% of their melting temperature (Reed, 2004). Although thermal-barrier coatings can be used to increase the application temperature, the component is still restricted by the melting point of the substrate, and for safety reasons the maximum attainable temperatures are still limited (Goward, 1998). If the operating temperatures could be increased, there would be a number of advantages. Higher temperatures improve the efficiency of turbine engines, enabling greater thrust, improved fuel efficiency and thus reduced pollution.

There is increasing interest in using a different alloy system with a much higher melting point. Intermetallic compounds have been considered because of their high-temperature strengths, but the inherent room-temperature brittleness of these materials remains problematic (Wolff and Sauthoff, 1996). One solution would be to base the new materials on alloys with high melting points and use the naturally-occurring precipitates of that system. This should also help keep the processing cost to a minimum. These systems would be similar in structure to the NBSAs with a matrix and a fine dispersion of small, preferably coherent, and hence stable, precipitates. Face-centred cubic (fcc) structures are advantageous because, being close-packed, they are more creep resistant. Refractory metals (*e.g.* Nb, Mo, and W) have been considered because of their high melting points (2477°C, 2623°C, and 3422°C respectively), but their more open body-centred cubic structures are more susceptible to creep, as well as being prone to rapid oxidation, even at relatively low temperatures (Briant, 1994). Platinum group metals (platinum, iridium, and rhodium) were targeted because they have high melting points, good environmental resistance, and a mostly fcc structure (Yamabe *et al.*, 1996; Wolff and Hill, 2000).

* *School of Chemical and Metallurgical Engineering, University of the Witwatersrand, Johannesburg, South Africa.*

† *African Materials Science and Engineering Network (AMSEM), a Carnegie-IAS Network.*

† *DST/NRF Centre of Excellence in Strong Materials, hosted by University of the University of the Witwatersrand, Johannesburg, South Africa.*

§ *Department of Mechanical and Manufacturing Engineering, University of Nairobi, Nairobi, Kenya.*

** *Advanced Materialls Division, Mintek, Randburg, Johannesburg, South Africa.*

∞ *School of Chemistry, University of the Witwatersrand, Johannesburg, South Africa.*

 ISSN 2225-6253. Paper received Oct. 2013; revised paper received Oct. 2014.

High-order additions to platinum-based alloys for high-temperature applications

Platinum-based alloys are being developed to have microstructures very similar to nickel-based superalloys for potential for high-temperature applications in aggressive environments (Wolff and Hill, 2000; Cornish *et al.*, 2009). Since the chemistries of nickel and platinum are similar, Pt-based alloys can be made with gamma prime ~Pt_3Al precipitates in a gamma (Pt) matrix. Although similar (Massalski, 1990), the Pt-Al phase diagram is more complicated than that of Ni-Al in that Pt_3Al has at least three variants, depending on the temperature, whereas Ni-Al has only one, the $L1_2$ phase, which is ordered fcc. In Pt-Al, the $L1_2$ phase is the highest temperature ~Pt_3Al phase, whereas the lower temperature ~Pt_3Al phases are tetragonal, and so less desirable for components subjected to ranges of temperature, although they can be stabilized by various additions. Currently, the Pt-Al-Cr-Ru system is one of the bases for developing Pt-based alloys, where Al allows the formation of the Pt_3Al precipitate and also gives protection by forming alumina scale, Cr provides oxidation resistance and stabilization for the $L1_2$ ~Pt_3Al phase, and Ru provides solid solution strengthening in the (Pt) matrix. Other researchers (Wenderoth *et al.*, 2005; Völkl *et al.*, 2009) have developed alloys based on Pt-Al-Cr-Ni.

In an investigation of some Pt-Al-Cr-Ru alloys, it was found that both Ru and Cr partition preferentially to the (Pt). The solubility ranges of Ru and Cr were found to be 0.5 to 0.7 at.% Ru and 1.3 to 1.8 at.% Cr in the precipitates, and between 1.2 to 2.4 at.% Ru and 2.7 to 4.6 at.% Cr for the (Pt) phase (Shongwe *et al.*, 2008, 2010). The best quaternary alloy in terms of high precipitate volume, microstructure, and hardness to date is ~Pt_{82}:Al_{12}:Cr_4:Ru_2 (at.%) (Shongwe *et al.*, 2008, 2010). It was postulated that a quinary addition to the optimum Pt-Al-Cr-Ru quaternary alloy could improve the melting temperature and stability and increase the volume fraction of ~Pt_3Al. This would improve mechanical properties, such as hardness and strength, at high temperatures while still retaining the oxidation and corrosion resistance in these aggressive environments.

It is well recognized (Cornish *et al.*, 2009) that Pt-based alloys have serious disadvantages due to their price and their density. Attempts are ongoing to substitute some of the Pt with another element, which is less expensive and less dense, but still retaining the high-temperature capabilities and the required microstructure. Addition of niobium to Pt-based alloys resulted in elevated strengths at high temperatures through precipitation-hardening (Wenderoth *et al.*, 2008), and since vanadium is near Nb in the periodic table and has a smaller atomic radius than Nb, it may also act as a precipitation strengthener in addition to solid solution strengthening. The binary phase diagrams of Nb-Pt and Pt-V have the melting point of (Pt) increasing with increasing additions of Nb and V respectively (Massalski, 1990). This could counteract the effect of the Al-Pt eutectic with the decreasing (Pt) melting point. In order to predict the effect of Nb and V on the Pt-based alloys, phase diagrams were studied for (which had not been reported before): Pt-Al-Nb (Ndlovu, 2006; Samal and Cornish, 2010) and Pt-Cr-Nb (Mulaudzi, 2009), as well as Pt-Al-V (Odera *et al.*, 2012a; Odera, 2013a) and Pt-Cr-V (Odera *et al.*, 2012b; Odera, 2013a). The results indicate how the additions affect the microstructure and give an idea of the maximum additions without losing the two-phase structure, or forming other phases.

Experimental procedure

Alloy buttons weighing ~2 g each were prepared for compositions chosen (Tables I and II) from previous work (Ndlovu, 2006; Shongwe *et al.*, 2008, 2010; Mulaudzi, 2009; Samal and Cornish, 2010; Odera *et al.*, 2012a, 2012b; Odera, 2013) for a series of alloys based on Pt-Al-Cr-Ru with additions of Nb and/or V. The elemental components had 99.9% purity, except for V (99.6% purity). The samples were manufactured by arc-melting under argon, on a water-cooled copper hearth, with Ti as an oxygen-getter, and each was turned over and re-melted three times in an attempt to

Table I

Composition analyses (at.%) for the as-cast alloys

Alloy	Pt	Al	Cr	Ru	V	Nb	Phase
1 $Pt_{63.9}$:$Al_{12.2}$:$Cr_{4.3}$:$Ru_{0.7}$:$V_{18.9}$	63.9±1.0	12.2±0.4	4.3±0.5	0.7±0.4	18.9±0.9	-	-
	65.2±0.7	5.0±1.1	4.9±0.2	1.4±0.3	23.5±0.7	-	(Pt)
	62.3±1.2	27.4±1.9	2.5±0.3	0	7.8±0.7	-	~Pt_3Al
2 $Pt_{69.5}$:$Al_{11.5}$:$Cr_{4.2}$:$Ru_{0.6}$:$V_{14.2}$	69.5±0.5	11.5±0.5	4.2±0.3	0.6±0.3	14.2±0.5	-	-
	70.2±1.4	8.4±1.1	4.4±0.3	1.0±0.6	16.1±1.1	-	(Pt)
	66.9±1.6	22.5±3.7	3.2±0.3	0	7.5±2.1	-	~Pt_3Al
3 $Pt_{75.2}$:$Al_{11.2}$:$Cr_{4.0}$:$Ru_{0.6}$:$V_{9.5}$	74.7±0.6	11.2±0.4	4.0±0.2	0.6±0.4	9.5±0.2	-	~Pt_3Al
4 $Pt_{78.7}$:$Al_{12.2}$:$Cr_{3.8}$:$Ru_{0.6}$:$V_{5.2}$	78.2±0.9	12.2±0.7	3.8±0.2	0.6±0.1	5.2±0.3	-	~Pt_3Al
5 $Pt_{63.2}$:$Al_{12.9}$:$Cr_{4.0}$:$Ru_{0.7}$:$V_{19.0}$:$Nb_{0.6}$	63.4±1.1	12.9±1.7	4.0±0.1	0.7±0.3	19.0±0.9	0.6±0.4	-
	62.7±0.6	6.3±0.6	5.1±0.4	1.0±0.4	23.3±0.9	1.6±0.7	(Pt)
	56.1±0.8	31.1±0.9	3.9±0.3	0.1±0.1	8.8±0.4	0	~Pt_3Al + (Pt) eutectic
6 $Pt_{71.7}$:$Al_{12.8}$:$Cr_{4.9}$:$Ru_{1.1}$:$V_{9.9}$:$Nb_{0.3}$	71.0±2.1	12.8±1.8	4.9±0.4	1.1±0.8	9.9±0.5	0.3±0.1	-
	73.8±1.6	8.8±2.0	4.5±0.4	1.0±0.8	10.9±1.3	1.1±0.8	(Pt)
	64.4±1.2	29.4±1.0	2.7±0.2	0	3.6±0.5	0	~Pt_3Al

Table II

Composition analyses (at.%) for the alloys heat treated at 1000°C for 1500h

Alloy	Pt	Al	Cr	Ru	V	Nb	Phase
1H	61.8±0.7	13.9±0.9	4.1±0.3	0.6±0.2	19.6±0.4	-	-
$Pt_{61.7}:Al_{13.9}:Cr_{4.1}:Ru_{0.6}:V_{19.6}$	61.8±1.3	7.1±1.3	4.7±0.2	1.4±0.4	25.0±1.4	-	~Pt_2V
	57.9±0.4	37.6±0.8	1.8±0.3	0	2.7±0.4	-	~Pt_3Al
2H	69.6±1.3	11.4±1.0	4.4±0.2	0.5±0.4	14.1±0.7	-	~Pt_3Al
$Pt_{69.8}:Al_{11.4}:Cr_{4.4}:Ru_{0.5}:V_{14.1}$							
3H	76.4±1.0	10.1±0.3	3.7±0.6	0.8±0.1	9.0±0.4	-	-
$Pt_{83.0}:Al_{10.1}:Cr_{3.7}:Ru_{0.8}:V_{9.0}$	75.8±1.0	10.4±0.6	4.3±0.3	0.8±0.2	8.7±0.3	-	~Pt_3Al
	75.8±2.0	10.5±1.4	4.2±0.5	0.5±0.1	9.0±0.4	-	~Pt_3Al
4H	82.5±0.7	8.7±0.6	3.7±0.4	0.8	4.3±0.6		-
$Pt_{83.0}:Al_{8.7}:Cr_{3.7}:Ru_{0.8}:V_{4.3}$	82.6±2.0	6.8±1.5	4.1±0.5	1.6±1.3	4.9±0.4		(Pt) with ~Pt_3Al pptn.
	80.4±2.0	10.1±1.7	3.9±0.4	1.2±0.8	4.4±0.5		~Pt_3Al with (Pt) pptn.
5H	53.4±1.8	18.0±1.4	4.3±0.3	1.4±0.9	21.9±1.3	1.0±0.8	-
$Pt_{53.9}:Al1_{8.0}:Cr_{4.3}:Ru_{1.4}:V_{21.9}:Nb_{1.0}$	56.4±1.6	8.1±1.9	5.1±0.5	2.2±0.6	26.9±0.3	1.3±0.8	~Pt_2V
	57.3±1.3	24.8±1.6	2.4±0.3	0.2	14.8±1.7	0.5±0.1	~Pt_3Al
	47.8±1.9	7.7±2.4	7.6±0.9	2.6±0.1	34.3±3.4	0	~PtV
	55.6±0.3	17.0±1.3	4.5±0.5	1.3±0.3	21.6±0.9	0	~PtV + ~Pt_2V
6H	73.9±0.6	11.5±0.6	4.5±0.3	0.5±0.2	9.3±0.3	0.3±0.1	~Pt_3Al
$Pt_{74.1}:Al_{11.5}:Cr_{4.5}:Ru_{0.5}:V_{9.3}:Nb_{0.3}$							

achieve homogeneity. The buttons were halved, and one half was prepared metallographically in the as-cast condition, with the other half being sealed in an evacuated ampoule, then annealed at 1000°C for 1500 hours and quenched in water, then similarly prepared.

The microstructures of all the alloys were analysed using a scanning electron microscope (SEM) model HR-NovaNano SEM200, using both secondary (SE) and backscattered electron (BSE) modes. An accelerating voltage of 20.0 kV was used on all the samples and the working distance ranged from 5.0 to 5.5 mm. Area and spot phase compositions were obtained from energy dispersive X-ray spectroscopy (EDX), taking an average of at least five different measurements in different places. The overall area from which composition measurements were taken was 1600 μm^2. The interaction volume of the X-rays can be as much as 3 μm across and deep (especially for higher atomic number elements and the necessary high accelerating voltage). Usually an accuracy of ±1 at.% would be expected for this technique. A Bruker D2 Phaser Diffractometer with Lynxeye detector using Co Kα radiation of wavelength 1.78897 Å was used for X-ray diffraction (XRD) to confirm the phase identities. The diffraction angles ranged between $2\theta = 20°$ to $2\theta = 100°$. The generator settings were 30 kV and 10 mA and the step size was 0.0260°.

Microhardness tests were performed after etching in a solution of 10 g NaCl in 100 cm^3 HCl (32% vol. concentration), using a DC power supply and a voltage range of 9 V to 12 V (Odera *et al.*, 2012c). A Vickers microhardness tester was used with a load of 300 g, and at least five measurements taken.

Results

There were losses during melting, especially of Ru (up to 1.5 at.%) and Nb (up to 1.7 at.%), even higher than before (Cornish *et al.*, 2009). The EDX results of the as-cast alloys are shown in Table I, whereas those of the heat-treated alloys are given in Table II. The last columns of Tables I and II show the phases that were confirmed by XRD analysis. Table III is a summary of the data from Rietveld analysis, while Table IV contains the hardness data.

$Pt_{63.9}:Al_{12.2}:Cr_{4.3}:Ru_{0.7}:V_{18.9}$ (at.%) (alloys 1 and 1H)

The as-cast $Pt_{63.9}:Al_{12.2}:Cr_{4.3}:Ru_{0.7}:V_{18.9}$ (at.%) alloy (Figure 1a) had dendrites of (Pt) in a matrix of ~Pt_3Al. The expected eutectic was not visible, but it could have been too fine to resolve. Vanadium partitioned preferentially to the (Pt) at ~23.5 at.% V compared to ~7.8 at.% V in ~Pt_3Al. After heat treatment, the (Pt) had transformed to ~Pt_2V (Figure 1b) and the overall composition changed slightly, with 0.1 at.% Ru lower content and 0.7 at.% V higher content (although the limit of the detector was ±1 at.%). The phase transformation was confirmed by XRD, as shown in Figure 2.

$Pt_{69.5}:Al_{11.5}:Cr4_{.2}:Ru_{0.6}:V_{14.2}$ (at.%) (alloys 2 and 2H)

The microstructure of as-cast $Pt_{69.5}:Al_{11.5}:Cr4_{.2}:Ru_{0.6}:V_{14.2}$ (at.%) was very similar to the previous alloy, and the grain boundaries were irregular (Figure 3a). Most of the V went into solution in the (Pt). After heat treatment, the alloy became mostly single-phase ~Pt_3Al, with very little change in overall composition, with Ru and V decreasing by 0.1 at.% as measured by EDX (Tables I and II), and the grain boundaries had become much smoother, indicating that the heat treatment temperature and duration had an effect on the microstructure (Figure 3b).

$Pt_{75.2}:Al_{11.2}:Cr_{4.0}:Ru_{0.6}:V_{9.5}$ (at.%) (alloys 3 and 3H)

The as-cast $Pt_{75.2}:Al_{11.2}:Cr_{4.0}:Ru_{0.6}:V_{9.5}$ (at.%) alloy differed from the other as-cast alloys in that it was single-phase ~Pt_3Al, which was confirmed by XRD. After heat treatment, the alloy was still single-phase and the grain boundaries had also become more regular and shorter.

Table III

Rietveld analyses of selected samples

Alloy	Phase	Proportion, %	Space group	Lattice parameter, Å
1	Pt_3Al	53.5	$Pm\bar{3}m$	a = 3.86255
$Pt_{63.9}:Al_{12.2}:Cr_{4.3}:Ru_{0.7}:V_{18.9}$	(Pt)	0.1	$Fm\bar{3}m$	a = 3.96781
	Pt_3V	46.4	$Pm\bar{3}m$	a = 3.87000
	RuAl	0.2	$Pm\bar{3}m$	a = 3.01516
1H	Pt_3Al	59.5	$Pm\bar{3}m$	a = 3.86742
$Pt_{61.7}:Al_{13.9}:Cr_{4.1}:Ru_{0.6}:V_{19.6}$	Pt_2V	36.2	*Immm*	a = 2.73018
				b = 8.27452
				c = 3.83065
	CrPt	4.3	*P213*	a = 4.85507
2	Pt_3Al	79.7	$Pm\bar{3}m$	a = 3.86255
$Pt_{69.5}:Al_{11.5}:Cr_{4.2}:Ru_{0.6}:V_{14.2}$	(Pt)	0.1	$Fm\bar{3}m$	a = 3.96796
	Pt_3V	19.5	$Pm\bar{3}m$	a = 3.87000
	RuAl	0.7	$Pm\bar{3}m$	a = 3.01639
2H	Pt_3Al	66.6	$Pm\bar{3}m$	a = 3.86362
$Pt_{69.8}:Al_{11.4}:Cr_{4.4}:Ru_{0.5}:V_{14.1}$	Pt_3V	18.6	$Pm\bar{3}m$	a = 3.81112
	Cr_3Pt	14.8	$Pm\bar{3}m$	a = 3.87362
4	Pt_3Al	90.28	$Pm\bar{3}m$	a = 3.87750
5	Pt_3Al	95.7	$P\bar{4}/mbm$	a = 5.47216
$Pt_{63.2}:Al_{12.9}:Cr_{4.0}:Ru_{0.7}:V_{19.0}:Nb_{0.6}$			$Fm\bar{3}m$	c = 7.74843
	(Pt)	1.4	$I\bar{4}/mmm$	a = 3.96532
	Pt_3V	2.1		a = 3.87182
			$Pm\bar{3}m$	c = 8.08972
	RuAl	0.8		a = 3.02034
5H	Pt_3Al	62.0	$P\bar{4}/mbm$	a = 5.39536
$Pt_{53.9}:Al_{18.0}:Cr_{4.3}:Ru_{1.4}:V_{21.9}:Nb_{1.0}$				c = 8.12855
	PtV	34.8	*Pmma*	a = 3.41466
				b = 2.70016
				c = 4.76353
	Pt_2V	3.2	*Immm*	a = 2.71709
				b = 8.32022
				c = 3.79396
6	Pt_3Al	94.1	$Pm\bar{3}m$	a = 3.88863
$Pt_{71.7}:Al_{12.8}:Cr_{4.9}:Ru_{1.1}:V_{9.9}:Nb_{0.3}$	Pt_3V	2.7	$Pm\bar{3}m$	a = 3.89561
	RuAl	3.2	$Pm\bar{3}m$	a = 3.03984

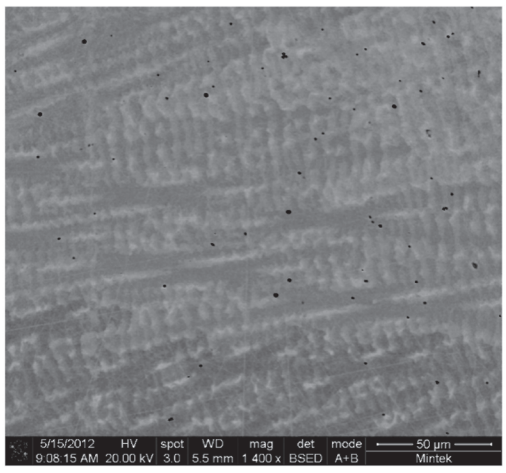

Figure 1a—SEM-BSE image of as-cast $Pt_{63.9}:Al_{12.2}:Cr_{4.3}:Ru_{0.7}:V_{18.9}$ (at.%), showing dark (Pt) and light ~Pt_3Al

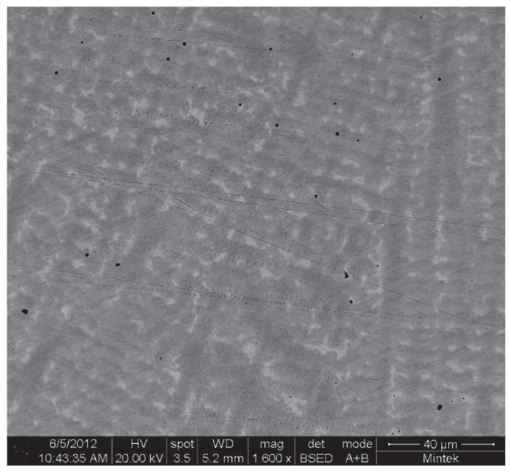

Figure 1b—SEM-BSE image of annealed $Pt_{61.7}:Al_{13.9}:Cr_{4.1}:Ru_{0.6}:V_{19.6}$ (at.%), showing a two-phase structure of dark ~Pt_2V and light ~Pt_3Al

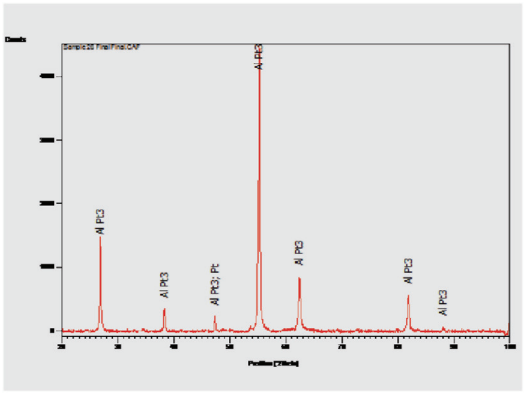

Figure 2a—XRD pattern for as-cast $Pt_{63.9}$:$Al_{12.2}$:$Cr_{4.3}$:$Ru_{0.7}$:$V_{18.9}$ (at.%), showing peaks for Pt and Pt_3Al

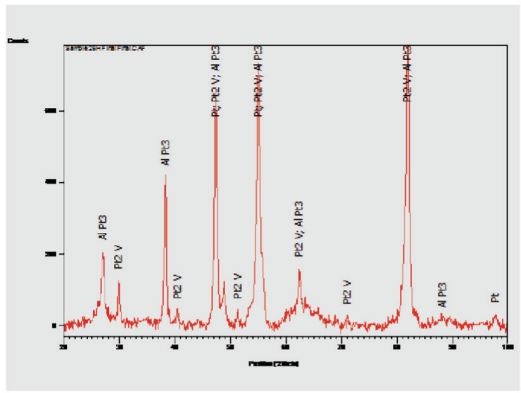

Figure 2b—XRD pattern for annealed $Pt_{63.9}$:$Al_{12.2}$:$Cr_{4.3}$:$Ru_{0.7}$:$V_{18.9}$ (at.%), showing peaks for Pt and ~Pt_2V

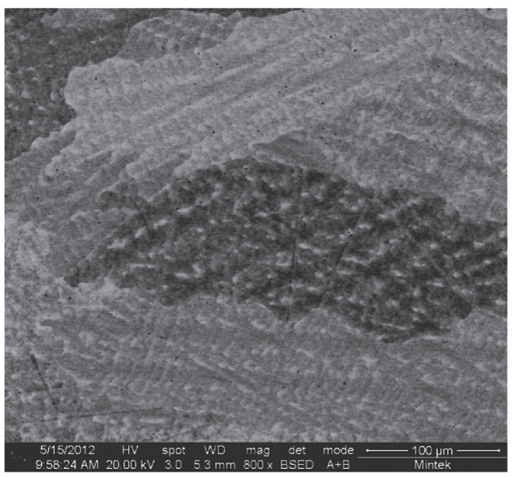

Figure 3a—SEM-BSE image of as-cast $Pt_{69.5}$:$Al1_{1.5}$:$Cr_{4.2}$:$Ru_{0.6}$:$V_{14.2}$ (at.%), showing dark ~Pt_3Al and light (Pt), with irregular grain boundaries

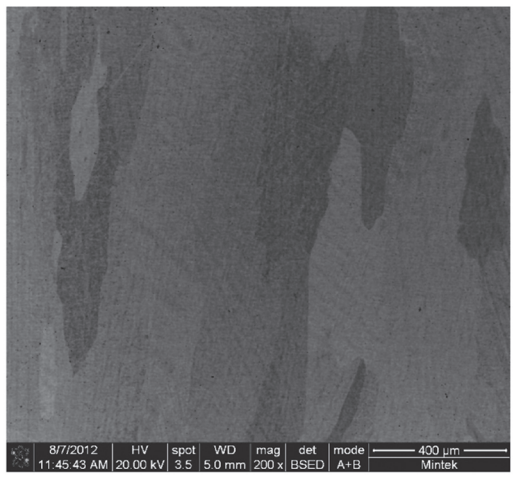

Figure 3b—SEM-BSE image of annealed $Pt_{69.8}$:$Al_{11.4}$:$Cr_{4.4}$:$Ru_{0.5}$:$V_{14.1}$ (at.%), showing mainly single-phase ~Pt_3Al with grains at different orientations

$Pt_{78.7}$:$Al_{12.2}$:$Cr_{3.8}$:$Ru_{0.6}$:$V_{5.2}$ (at.%) (alloys 4 and 4H)

Similar to the previous alloy, Figure 4a shows that as-cast $Pt_{78.7}$:$Al_{12.2}$:$Cr_{3.8}$:$Ru_{0.6}$:$V_{5.2}$ (at.%) was single-phase ~Pt_3Al, as confirmed by XRD. The different contrasts are due to orientation (Cornish *et al.*, 2008), since the analyses were within 2 at.% of each other. After heat treatment, the alloy had lost some Cr and V and was two-phase, with each phase containing precipitates of the other phase, which brought the analysed compositions closer together (Figure 4b). However, the low contrast between the phases made the microstructure difficult to discern. The (Pt) phase had higher Pt, Ru, and V with lower Al, and unlike the other samples, (Pt) was the lighter phase because it contained less V. The solid-state precipitations indicated retreating solvi of ~Pt_3Al and (Pt) with decreasing temperature.

$Pt_{63.2}$:$Al_{12.9}$:$Cr_{4.0}$:$Ru_{0.7}$:$V_{19.0}$:$Nb_{0.6}$ (at.%) (alloys 5 and 5H)

The microstructure of as-cast $Pt_{63.2}$:$Al_{12.9}$:$Cr_{4.0}$:$Ru_{0.7}$:$V_{19.0}$:$Nb_{0.6}$ (at.%) (Figure 5a) was similar to that of the ternary alloy of average composition $Pt_{59.1}$:$Al_{23.1}$:$V_{17.8}$ (at.%) (reported as alloy 2 (Odera, 2013)), with the dendrites being (Pt) of higher Pt, Ru, and V and lower Al content, with a ~Pt_3Al + (Pt) eutectic. Although the targeted Nb content was 5 at.%, Nb was lost during melting, resulting in an average content of only 0.6 at.%. After annealing, the structure was much more complex (Figure 5b), and the composition was also slightly different. The (Pt) phase had transformed to ~Pt_2V and ~PtV (although its composition was fairly similar to the τ1 ternary phase of Pt-Al-V (Odera, 2013). These phases were interpreted as a coarsened eutectoid. The XRD patterns of the as-cast and annealed samples are shown in Figure 6, and Table III contains the data for Rietveld refinement. The pattern after Rietveld refinement is shown in Figure 6c.

$Pt_{71.7}$:$Al_{12.8}$:$Cr_{4.9}$:$Ru_{1.1}$:$V_{9.9}$:$Nb_{0.3}$ (at.%) (alloys 6 and 6H)

Figure 7a shows the two-phase microstructure of as-cast $Pt_{71.7}$:$Al_{12.8}$:$Cr_{4.9}$:$Ru_{1.1}$:$V_{9.9}$:$Nb_{0.3}$ (at.%). After annealing (Figure 7b), the alloy was single-phase ~Pt_3Al.

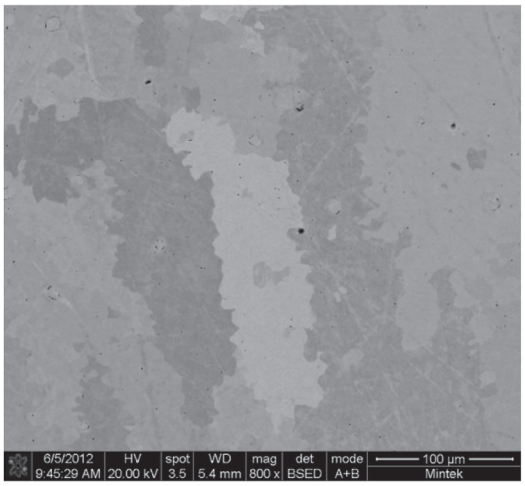

Figure 4a—SEM-BSE image of as-cast $Pt_{78.7}$:$Al_{12.2}$:$Cr_{3.8}$:$Ru_{0.6}$:$V_{5.2}$ (at.%), showing single- phase ~Pt_3Al, with irregular grains at different orientations

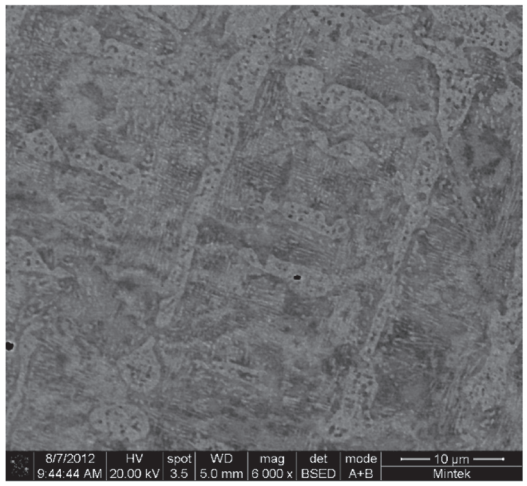

Figure 4b—SEM-BSE image of annealed $Pt_{83.0}$:$Al_{8.7}$:$Cr_{3.7}$:$Ru_{0.8}$:$V_{4.3}$ (at.%), showing light (Pt) and dark ~Pt_3Al

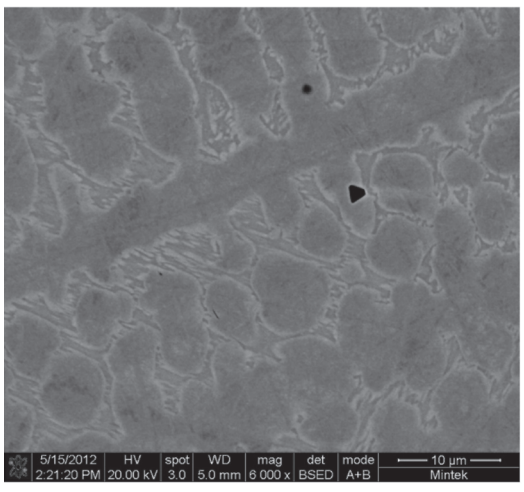

Figure 5a—SEM-BSE image of as-cast $Pt_{63.2}$:$Al_{12.9}$:$Cr_{4.0}$:$Ru_{0.7}$:$V_{19.0}$:$Nb_{0.6}$ (at.%), showing dark (Pt) dendrites and a eutectic of ~Pt_3Al + (Pt)

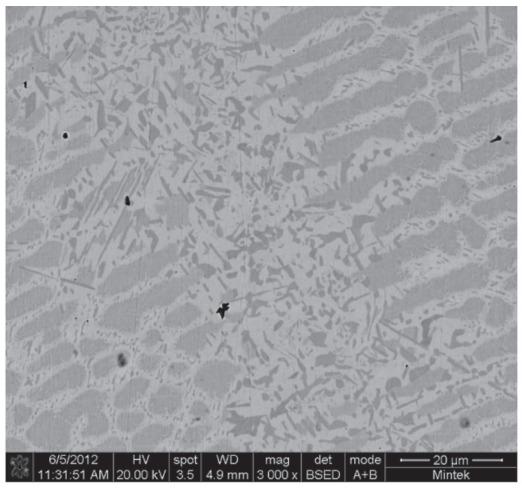

Figure 5b—SEM-BSE image of annealed $Pt_{53.9}$:$Al_{18.0}$:$Cr_{4.3}$:$Ru_{1.4}$:$V_{21.9}$:$Nb_{1.0}$ (at.%), showing medium ~Pt_2V with a light solid-state precipitate, dark ~PtV, coarsened eutectoid of ~PtV + ~Pt_2V

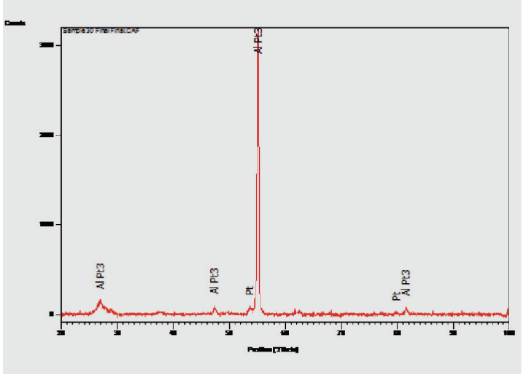

Figure 6a—XRD pattern of $Pt_{63.2}$:$Al_{12.9}$:$Cr_{4.0}$:$Ru_{0.7}$:$V_{19.0}$:$Nb_{0.6}$ (at.%), showing peaks for (Pt) and ~Pt_3Al

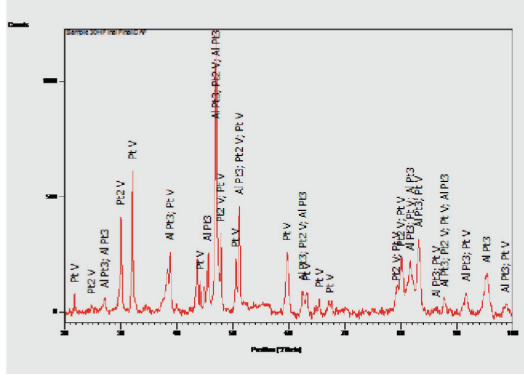

Figure 6b—XRD pattern of annealed $Pt_{53.9}$:$Al_{18.0}$:$Cr_{4.3}$:$Ru_{1.4}$:$V_{21.9}$:$Nb_{1.0}$ (at.%), showing peaks for Pt_3Al, PtV, and Pt_2V

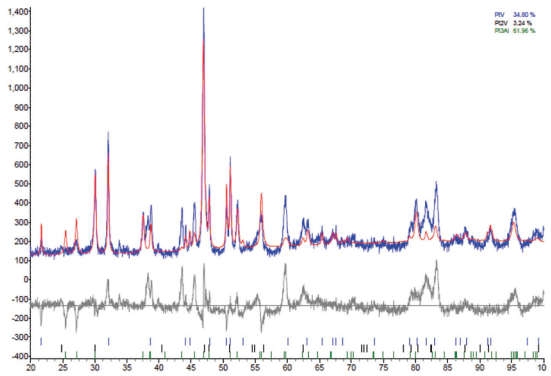

Figure 6c—The pattern after Rietveld refinement for annealed alloy 5H, $Pt_{53.9}$:$Al_{18.0}$:$Cr_{4.3}$:$Ru_{1.4}$:$V_{21.9}$:$Nb_{1.0}$ (at.%), confirming the presence of ~Pt_3Al, ~PtV, and ~Pt_2V

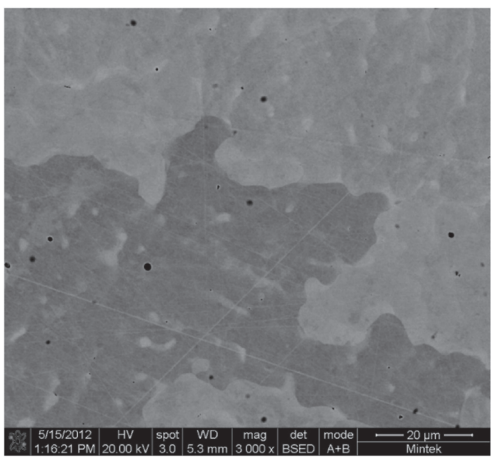

Figure 7a—SEM-BSE image of as-cast $Pt_{71.7}$:$Al_{12.8}$:$Cr_{4.9}$:$Ru_{1.1}$:$V_{9.9}$:$Nb_{0.3}$ (at.%) showing dark ~Pt_3Al and light (Pt), with variations in contrast also due to orientation

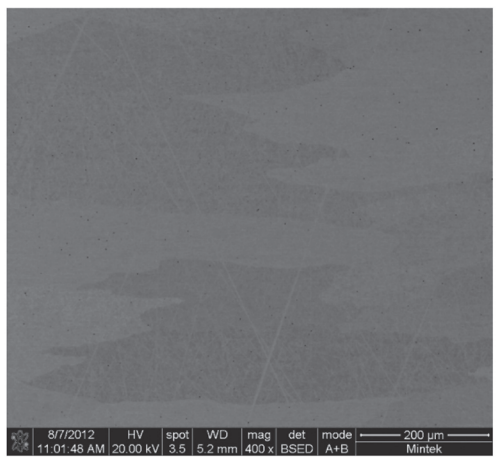

Figure 7b—SEM-BSE image of annealed $Pt_{74.1}$:$Al_{11.5}$:$Cr_{4.5}$:$Ru_{0.5}$:$V_{9.3}$:$Nb_{0.3}$ (at.%), showing single-phase ~Pt_3Al with grains at different orientations

Rietveld Analyses

Due to the complexity of the XRD spectra and the difficulty in resolving peaks of the different phases, which were very close, Rietveld analysis was done. The phases identified by XRD are shown in Tables I and II, and the Rietveld analysis data is given in Table III. Obviously, the Rietveld data was more accurate (even though alloy 4 contained only one phase, and this was not 100%), and sometimes detected phases that had been overlooked by XRD. This was particularly useful for the lower temperature phases that form from (Pt) and have similar peaks.

In alloy 1, XRD analysis confirmed the presence of ~Pt_3Al and (Pt). After Rietveld refinement, the phases identified were ~Pt_3Al, ~Pt_3V, and traces of (Pt) and RuAl. The solid solution must have gone through a solid-state transformation to form ~Pt_3V, which could not be identified by XRD.

In Alloy 1H, both XRD and Rietveld analyses identified both ~Pt_3Al and ~Pt_2V. However, Rietveld also indicated the presence of a small amount of CrPt.

In alloy 2, XRD analysis identified ~Pt_3Al and (Pt) while Rietveld analysis identified ~Pt_3Al, and ~Pt_3V with only traces of (Pt) and RuAl. The (Pt) identified by XRD must have gone through solid-state transformation to form ~Pt_3V.

In alloy 2H, XRD analysis identified only ~Pt_3Al peaks. Rietveld analysis confirmed the presence of ~Pt_3Al and also identified smaller amounts of ~Pt_3V and ~Cr3Pt.

In alloy 4, XRD identified ~Pt_3Al and this was confirmed by Rietveld analysis. There were smaller amounts of other phases, since Rietveld analysis gave the proportion of the ~Pt_3Al as 90.28%.

In Alloy 5, XRD analysis identified ~Pt_3Al and (Pt). Rietveld analysis confirmed the presence of ~Pt_3Al and also identified smaller amounts of ~Pt_3V and (Pt). This shows that the alloy was predominantly ~Pt_3Al and some of the (Pt) went through solid-state transformation to form ~Pt_3V.

In alloy 5H, XRD analysis identified ~Pt_3Al, ~PtV, and ~Pt_2V, and the same phases were found by Rietveld analysis.

In alloy 6, XRD analysis identified ~Pt_3Al and (Pt) while Rietveld analysis found that the alloy was predominantly ~Pt_3Al (94.1%) with small amounts of ~Pt_3V (2.7%) and RuAl (3.2%). The solid solution identified by XRD analysis must have gone through solid-state transformation to form ~Pt_3V.

Hardness

There were no cracks or noticeable slip lines around the edges of the indentations (probably due to the low load of 300 g), although pincushioning was observed for as-cast alloys 2 and 5. Pincushioning results from sinking of the metal around the flat faces of the pyramid indenter, and gives an overestimate of the diagonal length, hence a lower hardness value. Alloy 1H had slight pincushioning in the annealed condition and again, there were no cracks or noticeable slip lines around the edges of the indentations. The hardness values are given in Table IV.

Half of the as-cast alloys had hardnesses above 500 $HV_{0.3}$. Alloy 5 had the highest hardness: 603 $HV_{0.3}$. As-cast alloys with ~Pt_3Al and (Pt) were generally harder than single-phase ~Pt_3Al, and these had higher V contents. The higher hardnesses could not be attributed to (Pt), which is softer, and pure platinum has a hardness of only ~50 HV (Murakami *et al.*, 2008). Only the alloys with higher V content had a two-phase structure of (Pt) and ~Pt_3Al. Thus, for the alloys studied, higher V content was the major contributing factor to higher hardness.

Figure 8 shows the variation of the hardnesses with vanadium content, indicating a general trend of increased hardness with vanadium content, for the four alloy compositions (four as-cast and three annealed alloys). Also, the hardnesses for the annealed alloys were generally higher than the as-cast alloys.

Discussion

As-cast alloys 1 and 2 both contained (Pt) dendrites and ~Pt_3Al, and V partitioned preferentially to the (Pt), with alloy 1 having ~23.5 at.% V in (Pt) compared to ~7.8 at.% V in ~Pt_3Al, and alloy 2 having ~16 at.% V in (Pt) compared to ~10 at.% V in ~Pt_3Al. Alloy 6 also contained (Pt) dendrites and ~Pt_3Al, with the V partitioned preferentially to (Pt). There was ~11 at.% V in (Pt) and ~3.5 at.% V in ~Pt_3Al. All of the Nb went into solution in (Pt). Alloy 5 had (Pt) dendrites and a ~Pt_3Al + (Pt) eutectic, with ~23 at.% V in the (Pt) dendrites and ~9 at.% V in the eutectic, and again, all of the Nb was in solution in the (Pt). Alloys 3 and 4 were both single-phase ~Pt_3Al, with all the vanadium being in solution in ~Pt_3Al (~10 at.% V in alloy 3 and ~5 at.% V in alloy 4). One reason why V was selected as an addition to Pt-Al-based alloys was its high solubility in the solid-solution (Pt). It was hoped that this would increase the solid solution strengthening, and this occurred, since the hardnesses were higher than for the ternary alloys with the (Pt) and ~Pt_3Al phases (Hill, 2001; Süss, 2007; Odera, 2013).

The alloy compositions were chosen to target two-phase microstructure analogues to NBSAs, although some of the results were unexpected. The (Pt) phase in as-cast alloy 1 transformed to ~Pt_2V during heat treatment (alloy 1H). Alloy 2H was two-phase (Pt) + ~Pt_3Al in the as-cast state (alloy 2), but became single-phase ~Pt_3Al after heat treatment.

Alloy 3H remained single-phase ~Pt_3Al after heat treatment, while alloy 4H changed from single-phase ~Pt_3Al (alloy 4) in the as-cast condition to two-phase ~Pt_3Al and (Pt), both with solid-state precipitation of the other phase, indicating sloping solvi for both phases. This would be beneficial for precipitation strengthening because it would potentially allow more precipitation and a higher volume fraction of precipitate to form.

The structure of alloy 5H changed substantially from that in the as-cast condition. The solid-solution (Pt), which had been part of a eutectic in the as-cast condition, transformed to two phases, ~PtV and ~Pt_2V, during heat treatment. There was also solid-state precipitation in the ~Pt_3Al dendrites. The morphology of the ~Pt_3Al component of the eutectic also became more rounded.

Alloy 6H, which had a two-phase structure in the as-cast condition, became single-phase ~Pt_3Al after heat treatment.

The required microstructure of fine precipitates of ~Pt_3Al

Figure 8—Hardness values ($HV_{0.3}$) plotted against vanadium content (at.%)

Table IV

Hardness values of as-cast and annealed alloys

Alloy no.	Average composition (at.%)	As-cast hardness ($HV_{0.3}$)	Annealed hardness ($HV_{0.3}$)	Phases present in the as-cast alloys	Phases present in the annealed alloys
1 & 1H	$Pt_{63.9}$:$Al_{12.2}$:$Cr_{4.3}$:$Ru_{0.7}$:$V_{18.9}$	537±13	700±20	~Pt_3Al, (Pt)	~Pt_3Al, ~Pt_2V
2 & 2H	$Pt_{69.5}$:$Al_{11.5}$:$Cr_{4.2}$:$Ru_{0.6}$:$V1_{4.2}$	428±11	482±24	~Pt_3Al, (Pt)	~Pt_3Al
3 & 3H	$Pt_{75.2}$:$Al_{11.2}$:$Cr_{4.0}$:$Ru_{0.6}$:$V_{9.5}$	377±8	359±9	~Pt_3Al	~Pt_3Al
4 & 4H	$Pt_{78.7}$:$Al_{12.2}$:$Cr_{3.8}$:$Ru_{0.6}$:$V_{5.2}$	422±9	-	~Pt_3Al	~Pt_3Al, (Pt)
5 & 5H	$Pt_{63.2}$:$Al_{12.9}$:$Cr_{4.0}$:$Ru_{0.7}$:$V_{19.0}$:$Nb_{0.6}$	603±21	821±32	~Pt_3Al, (Pt)	~Pt_3Al, ~PtV, ~Pt_2V
6 & 6H	$Pt_{71.7}$:$Al_{12.8}$:$Cr_{4.9}$:$Ru_{1.1}$:$V_{9.9}$:$Nb_{0.3}$	545±12	535±15	~Pt_3Al, (Pt)	~Pt_3Al

in a matrix of (Pt) is obtained only when an alloy solidifies to (Pt), and solid-state precipitation of ~Pt_3Al follows upon cooling, because the alloy is then in the (Pt) + ~Pt_3Al two-phase region, due to the sloping (Pt) solvus. Any other phases, especially a eutectic, that could also be associated with shrinkage porosity, could be detrimental, leading to reduced strength and toughness (Cornish *et al.*, 2009). All the alloys solidified with either (Pt) dendrites or single-phase ~Pt_3Al, and annealing did not always produce the required (Pt) + ~Pt_3Al precipitates. Thus, the compositions and/or the annealing procedure were unsuitable, because single-phase (Pt) was not formed on casting, although it might be expected that some eutectic would form because of the high cooling rates from arc-melting.

Alloy 1 had the highest V content, 19 at.%, and although it retained a two-phase structure after annealing, the (Pt) transformed to ~Pt_2V, which is not desirable. The V content was therefore too high. The next highest V content was in alloy 27, at ~15 at.%. This was also two-phase, with ~Pt_3Al dendrites and (Pt), but transformed to single-phase ~Pt_3Al on annealing, showing that the composition was too close to ~Pt_3Al. It is possible that a V content around ~15 at.% would produce the targeted microstructure. For the alloys that had single-phase ~Pt_3Al, rather than (Pt) dendrites, it was apparent that V additions effectively moved the overall alloy composition to the ~Pt_3Al liquidus surface, so that future higher order alloys should have lower Al contents to position them on the (Pt) liquidus surface.

The six alloys were based on the quaternary alloy Pt_{82}:Al_{12}:Cr_4:Ru_2 (at.%), and both V and Nb were added to replace Pt, while the contents of the other elements were meant to remain constant. However, because of losses during melting, the alloy compositions were not necessarily those targeted (hence the actual average compositions were used to designate the alloys). After heat treatment at 1500°C for 18 hours followed by water quenching, then further heat treatment at 1100°C for 12 hours followed by air cooling, the hardness of alloy Pt_{82}:Al_{12}:Cr_4:Ru_2 (at.%) was 378 HV10 with a 10±5% precipitate volume (Shongwe *et al.*, 2008, 2010) (measured by the grid method on enlarged micrographs). This shows that the addition of V, and in the case of alloys 5 and 6, V and Nb, substantially increased the hardness and possibly the precipitate volume fraction, even in the as-cast condition.

There was a general increase in the hardnesses after annealing, except for alloy 6H, which had the same value statistically, and alloy 3H, the hardness of which decreased marginally. The hardness of alloy 1 increased from 537 $HV_{0.3}$ to 700 $HV_{0.3}$ (alloy 1H), which was expected since the (Pt) solid solution in the as-cast alloy transformed to ~Pt_2V during annealing. As-cast alloy 2 was two-phase ~Pt_3Al and (Pt), but became single-phase ~Pt_3Al on annealing (alloy 2H), and the hardness increased from 428 $HV_{0.3}$ to 482 $HV_{0.3}$. As-cast alloy 3 was single-phase ~Pt_3Al, and remained single-phase after annealing (alloy 3H), with the hardness remaining the same. As-cast alloy 4 was single-phase ~Pt_3Al, but became two-phase ~Pt_3Al and (Pt) after annealing and disintegrated on further metallographic preparation, indicating brittleness and probable associated increased hardness. Alloy 5 had two phases, ~Pt_3Al and (Pt), in the as-cast condition but during annealing (alloy 5H), (Pt) transformed to ~PtV and ~Pt_2V. Consequently, the hardness increased from 603 $HV_{0.3}$ to 821 $HV_{0.3}$ because of the two Pt-V intermetallic compounds. The as-cast alloy 6 had two phases, ~Pt_3Al and (Pt), which changed to single-phase ~Pt_3Al during annealing, although the hardness remained the same, taking the errors in the hardnesses into account (Table IV).

The as-cast alloys did not have the expected microstructure, although they were generally harder than the quaternary alloys (Shongwe *et al.*, 2008, 2010; Odera, 2013), where the hardest alloy was Pt_{84}:Al_{11}:Cr_3:Ru_2 (at.%) with a hardness of 472 HV_{10}. They were also harder than the eight ternary Pt-Al based alloys investigated by Hill (2001), where the hardest alloy had a Vickers hardness of 530 HV. However, Pt-Al-V (Odera *et al.*, 2012a; Odera, 2013) and Pt-Cr-V alloys (Odera *et al.*, 2012b; Odera, 2013) and Pt-Al-Cr alloys (Süss, 2007) were generally much harder than the current as-cast alloys, because many of the Pt-Al-V and Pt-Cr-V alloys contained the hard Pt-V intermetallic phases. The high hardness of some of the Pt-Al-Cr alloys was attributed to ~$PtAl_2$, ~PtAl, and ~Pt_2Al_3. The Pt-Cr-Ru system (Süss, 2004) exhibited hardnesses between 225±13 for (Pt) and 1013±68 for an alloy with A15 Cr_3Pt. The latter sample showed cracking around the indentations, which is detrimental – however, this was not seen in the current alloys. Thus, although the current alloys did not all attain the desired ~Pt_3Al - (Pt) microstructure, the phases were such that the alloys had reasonably high hardnesses without being brittle. El-Bagoury (2011) measured hardness of aged experimental NBSAs, solution-treated at 1120°C and 1180°C then aged at 845°C for 24 hours; the Vickers hardness for the specimens solution treated at 1120°C was 472 HV and for those at 1180°C were 450 HV. These values compare very well with those of the current alloys.

The heat treatment at 1000˚C for 1500 hours did not transform the higher order alloys to the intended structure of fine ~Pt_3Al precipitates in a matrix of (Pt), and in some cases full homogenization was not achieved, as shown by the large errors in the EDX analyses. It is suggested that a heat treatment similar to that of Wenderoth *et al.* (2005) be used, with two stages (under flowing argon). Thus, homogenization would be more achievable at a higher temperature of 1500˚C for a shorter period of 12 hours, followed by water quenching. The second step would result in precipitation: 1000˚C for 120 hours, also followed by water quenching.

Conclusions

There were some losses of Ru and Nb, so not all of the targeted compositions were made. It is possible to obtain two-phase structures of (Pt) and ~Pt_3Al with additions of V and Nb, although the microstructures still need to be optimized. The optimum addition of V is ~15 at.%; higher additions would result in the formation of the brittle intermetallic phases of the Pt-V system, but the effect of Nb could not be evaluated since the losses were too high. The hardnesses of the alloys investigated were higher than those of the quaternary Pt-based alloys previously investigated. The alloys therefore show promise in terms of both microstructure and hardness, and future work on alloys of different compositions would be beneficial.

High-order additions to platinum-based alloys for high-temperature applications

Recommendations

It is recommended that the Al content be reduced with addition of V to the higher order alloys to achieve the required microstructure of ~Pt_3Al precipitates within (Pt).

A two-step heat treatment, with a shorter time at 1500˚C for solution treatment, and a longer time at 1000˚C, is recommended.

References

Briant, C.L. 1994. High-temperature silicides and refractory alloys. *Materials Research Society Symposium Proceedings 322*. Briant, C.L., Petrovic, J.J., Belaway, B.P., Vasudevan, A.K., and Lipsitt, H.A. (eds.). Pittsburg. p. 305.

Cornish, L.A., Süss, R., Douglas, A., Chown, L.H., and Glaner L. 2009. The Platinum Development Initiative. Platinum-based alloys for high temperature and special applications: Part I. *Platinum Metals Review*, vol. 53, no. 1. pp. 2–10.

Cornish, L.A., Witcomb, M.J., Coetzee, S., Tshawe W., and Prins, S. 2008. Anomalies and pitfalls in phase analyses using BSE. *Proceedings of the Microstructural Society of Southern Africa*, Gaborone, Botswana, 23–25 July 2008. Vvol. 38, p. 9.

El-Bagoury, N. 2011. Microstructure and mechanical properties of aged nickel base superalloy. *Archives of Applied Science Research*, vol. 3, no. 2. pp. 266–276.

Goward, G.W. 1998. Progress in coatings for gas turbine airfoils. *Surface Coatings Technology*, vol. 108–109. pp. 73–79.

Hill, P.J. 2001. Superalloy analogues based on platinum for ultra-high temperature applications. PhD thesis, University of the Witwatersrand, South Africa.

Massalski, T.B. 1990. *Binary Alloy Phase Diagrams*. vol. 1, 2nd edn. ASM International, Materials Park, OH.

Mulaudzi, F.M. 2009, Constitution of the Pt-Cr-Nb system. MSc dissertation, University of the Witwatersrand, South Africa.

Murakami, T., Sahara, R., Harako, D., Akiba, M., Narushima, T., and Ouchi, C. 2008. Effect of solute elements on hardness and grain size in platinum based binary alloys. *Materials Transactions*, vol. 49, no. 3. pp. 538–547.

Ndlovu, G.F. 2006. Microstructural investigation of the Pt-Al-Nb system. MSc dissertation, University of the Western Cape, South Africa.

Odera, B.O. 2013. Addition of vanadium and niobium to platinum-based alloys. PhD thesis, University of the Witwatersrand, South Africa.

Odera, B.O., Cornish, L.A., Papo M.J., and Rading G.O. 2012c. Electrolytic etching of platinum-aluminium based alloys. *Platinum Metals Review*, vol. 56, no. 4. pp. 257–261.

Odera, B.O., Cornish, L.A., Papo, M.J., and Rading G.O. 2012b. Microstructural investigation of some as-cast alloys of the Pt-Cr-V system. *Proceedings of the Ferrous and Base Metals Development Network Conference*, Magaliesburg, South Africa, 15–17 October 2012. pp. 291–308.

Odera, B.O., Cornish, L.A., Shongwe, M.B., Rading, G.O., and Papo, M.J. 2012a. As-cast and heat-treated alloys of the Pt-Al-V system at the Pt-rich corner. *Journal of the Southern African Institute of Mining and Metallurgy,* vol. 112, no. 7. pp. 505–515.

Reed, R.C. 2008. The Superalloys: Fundamentals and Applications. Cambridge University Press.

Samal, S. and Cornish, L.A. 2010. Characterisation of the Pt-rich alloys in the Pt-Al-Nb system. *Proceedings of the Microstructural Society of Southern Africa,* Bela Bela, South Africa, 26–29 October 2010. vol. 40. p. 50.

Shongwe, B.M., Cornish, L.A., and Süss, R. 2008. Improvement of ~Pt_3Al volume fraction and hardness in a Pt-Al-Ru-Cr Pt-based superalloy. *Advanced Metals Initiative Conference*, Johannesburg, South Africa, 18–19 November 2004. Southern African Institute of Mining and Metallurgy, Johannesburg [on CD].

Shongwe, M.B., Odera, B., Samal, S., Ukpong, A.M., Watson, A., Süss, R., Chown, L.H., Rading G.O., and Cornish, L.A. 2010. Assessment of microstructures in the development of Pt-based superalloys. *Advanced Metals Initiative Light Metals Conference*, Johannesburg, 27–29 October 2010. Southern African Institute of Mining and Metallurgy, Johannesburg. Paper 184-202 Shongwe [on CD].

Süss, R. 2004. Investigation of the Pt-Cr-Ru system. MSc dissertation, University of the Witwatersrand, South Africa.

Süss, R. 2007. Investigation of the Pt-Al-Cr system as part of the development of the Pt-Al-Cr-Ru thermodynamic database. PhD thesis, University of the Witwatersrand, South Africa.

Völkl, R., Wenderoth, M., Preussner, J., Vorberg, S., Fischer, B., Yamabe-Mitarai, Y., Harada, H., and Glatzel, U. 2009. Development of a precipitation-strengthened Pt-based superalloy. *Materials Science and Engineering A*, vol. 510–511A. pp. 328–331.

Wenderoth M., Cornish L.A., Süss R., Vorberg S., Fischer B., Glatzel U., and Völkl, R. 2005. On the development and investigation of quaternary Pt-based superalloys with Ni additions. *Metallurgical and Material Transactions A*, vol. 36A. pp. 567–575.

Wenderoth, M., Voberg, S., Fischer, B., Yamabe-Mitarai, Y., Harada, H., Glatzel, U., and Völkl, R. 2008. Influence of Nb, Ta, and Ti on microstructure and high-temperature strength of precipitation-hardened Pt-based alloys. *Materials Science and Engineering A*, vol. 483–484A. pp. 509–511.

Wolff, I.M. and Hill, P.J. 2000. Platinum metals-based intermetallics for high temperature service. *Platinum Metals Review*, vol. 44, no. 4. pp. 158–166.

Wolff, I.M. and Sauthoff, G. 1996. High temperature behaviour of precious metal base composites. *Metallurgical and Materials Transactions A*, vol. 27A. pp. 2642–2652.

Yamabe, Y., Koizumi, Y., Murakami, H., Ro, Y., Maruko, T., and Harada, H. 1996. Development of Ir-base refractory superalloys. *Scripta Materialia*, vol. 35, no. 2. pp. 211–215. ◆